Simulation of recurring earthquakes along the Nankai trough and their relationship to the Tokai long-term slow slip events taking into account the effect of locally elevated pore pressure and subducting ridges

Fuyuki Hirose[1] and Kenji Maeda[1]

Received 21 February 2013; revised 8 July 2013; accepted 9 July 2013; published 6 August 2013.

[1] Many earthquakes of moment magnitudes greater than 8 associated with subduction of the Philippine Sea plate under Japan have occurred along the Nankai trough with a recurrence interval of 90–150 years. A large-scale rupture of the Tokai fault segment is believed to be imminent because that segment did not rupture during the most recent Tonankai earthquake in 1944. Recurring long-term slow slip events (LSSEs) have recently been observed in the Tokai region. To investigate the current stress state in the Tokai region, we numerically simulated earthquake cycles using a three-dimensional model consisting of triangular cells based on the rate- and state-dependent friction law. Our numerical simulations successfully modeled the Tokai segment not ruptured during the 1944 Tonankai earthquake as well as the recurring LSSEs in the Tokai region. We found that a large characteristic displacement (L) and effective normal stress (σ) in areas of subducted ridges are essential to avoid rupture of the Tokai segment during the 1944 Tonankai earthquake. We also demonstrated that we can reproduce the recurring LSSEs by assigning low values of σ and L to the area beneath Lake Hamana without introducing a velocity-strengthening friction law at high slip rate. Our simulation showed that the amplitudes of the LSSEs increased following the earthquakes that did not rupture the Tokai segment, which suggests that the recent LSSEs may be related to the accumulation of stresses in the Tokai segment because it did not rupture during the 1944 earthquake.

Citation: Hirose, F., and K. Maeda (2013), Simulation of recurring earthquakes along the Nankai trough and their relationship to the Tokai long-term slow slip events taking into account the effect of locally elevated pore pressure and subducting ridges, *J. Geophys. Res. Solid Earth*, *118*, 4127–4144, doi:10.1002/jgrb.50287.

1. Introduction

[2] The Philippine Sea plate is subducting beneath southwestern Japan in a west-northwest direction at a rate of 1.5–6.5 cm/y (Figure 1) [*Heki and Miyazaki*, 2001]. The Nankai trough is the source area of large earthquakes associated with subduction of the Philippine Sea plate. The trough has been divided into the Nankai, Tonankai, and Tokai segments (Figure 1). Although the recurrence interval for earthquakes on these segments is 90−150 years [*Earthquake Research Committee*, 2001], earthquakes do not always involve all three segments (Figure 2). There is considerable concern that a large earthquake involving the Tokai segment will occur this century, because it did not rupture during the 1944 Tonankai earthquake (Figure 2) [e.g., *Ishibashi*, 1976]. The rupture of the 1944 Tonankai earthquake, initiated off Kii Peninsula, propagated northeastward [*Ichinose et al*., 2003; *Kikuchi et al*., 2003], and terminated off Tokai in an area where seismic survey data from active source have revealed subducted seafloor ridges (Figure 1) [*Kodaira et al*., 2004]; thus, the Tokai segment did not rupture in 1944, although the slower subducting rate along the Tokai segment may also contribute to the longer recurrence interval there.

[3] There are some simulation studies based on the rate- and state-dependent friction (RSF) law [*Dieterich*, 1979, 1981; *Ruina*, 1983] that dealt with subducted ridges or seamounts by assigning an additional effective normal stress (σ) and/or characteristic displacement (L) (see equation (3) in section 2.1) [e.g., *Honkura et al*., 1999; *Hori*, 2006; *Hirose et al*., 2009; *Yang et al*., 2012]. *Honkura et al*. [1999] conducted a numerical simulation of earthquakes at the Suruga trough in the Tokai area and showed that a significant preseismic sliding occurs in regions where locally large σ are applied in the seismogenic zone in the 2-D model, although they did not clearly describe about L. *Hori* [2006] applied locally large σ and L to the region of subducted seafloor ridges in the 3-D planar subduction model based on the

[1]Seismology and Volcanology Research Department, Meteorological Research Institute, Tsukuba, Japan.

Corresponding author: F. Hirose, Seismology and Volcanology Research Department, Meteorological Research Institute, 1-1 Nagamine, Tsukuba, Ibaraki 305-0052, Japan. (fhirose@mri-jma.go.jp)

2169-9313/13/10.1002/jgrb.50287

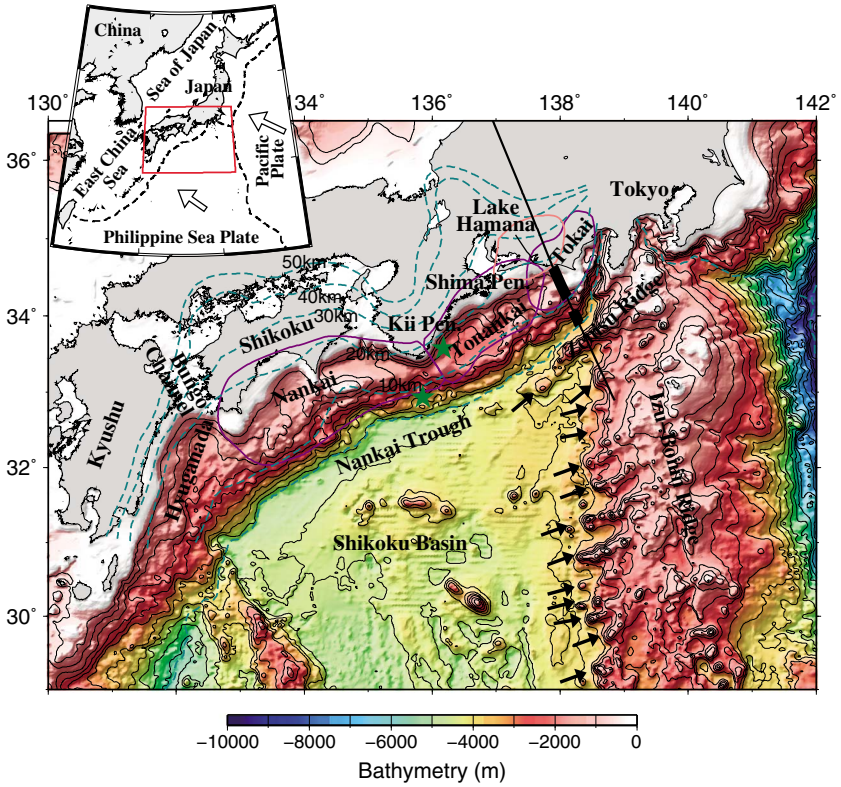

Figure 1. Bathymetric map off southern Japan. Green stars denote epicenters of the 1944 Tonankai and the 1946 Nankai earthquakes. Areas enclosed by purple lines represent the postulated source regions of Tokai earthquakes [*Central Disaster Management Council*, 2001], and Tonankai and Nankai earthquakes [*Earthquake Research Committee*, 2001]. The area enclosed by a pink line near Lake Hamana delineates the Tokai slow slip area, where the observed slip rate on the plate interface during 2001–2005 was more than 1 cm/yr [*Geographical Survey Institute*, 2007]. Broken blue lines are contours of depth to the top of the subducting Philippine Sea plate [*Hirose et al*., 2008b]. The straight black line marks a seismic reflection and refraction survey line; the thick parts of this line indicate locations of subducted ridges interpreted from the seismic data from active source [*Kodaira et al*., 2004]. Black arrows show the locations of ridges identified from bathymetric data. White arrows on the inset map indicate the direction of movement of the Pacific and Philippine Sea plates relative to the land plate [*Seno et al*., 1996; *Heki and Miyazaki*, 2001].

RSF law with composite law for state evolution including the saturation velocity, and reproduced the nonruptured Tokai segment. *Hirose et al*. [2009] set locally large L near the subducting ridges off Tokai and found that large L played a role in suppressing seaward spreading of the slow slips. However, their model was unable to simulate the lack of rupture of the Tokai segment in 1944 because of the limitations of their study area in the later description. *Yang et al*. [2012] showed in a 2-D model that introducing a large σ (and L) patch in velocity-weakening region arrested seismic rupture or enhanced seismic magnitude depending on the position of applied large σ (and L). Note that in their model, the large σ corresponds to the large L because they used a fixed value of h^* (see section 2.2). These results indicate that introducing a large σ and/or large-L patch in velocity-weakening region has the possibility to produce a barrier against seismic rupture.

[4] By the way, long-term slow slip events (LSSEs), which are events with durations of a few years, have been recorded recently in the Tokai region [*Ozawa et al*., 2002; *Ohta et al*., 2004; *Miyazaki et al*., 2006; *Geographical Survey Institute*, 2007]. The most recent event was observed via a dense GPS network and lasted from 2001 to 2005 with an average slip rate of 5 cm/y and a moment magnitude of 7.1 [*Geographical Survey Institute*, 2007]. Similar events, probably of smaller magnitude, with a recurrence interval of about 10−30 years have been observed beneath Lake Hamana (Figure 1) on the basis of electro-optical distance measurements [*Kimata and Yamauchi*, 1998], tilt change, and microseismic quiescence [*National Research Institute for Earth Science and Disaster Prevention*, 2004], tidal change [*Kobayashi and Yoshida*, 2004], and leveling surveys [*Sagiya et al*., 2007]. *Hirose et al*. [2008b] and *Matsubara et al*. [2008] estimated seismic velocity structures beneath southwestern Japan and found that the area where LSSEs were observed corresponds to a high *Vp/Vs* region along the Philippine Sea slab, which suggests that LSSEs may occur in the environment high pore fluid pressure probably resulting from dehydration of the Philippine Sea slab.

[5] *Kuroki et al*. [2004] and *Hirose et al*. [2009] attempted to simulate recurring LSSEs that precede cyclic great earthquakes in the Tokai region by using a three-dimensional earthquake cycle model based on the simple RSF law with the slip law for state evolution [*Dieterich*, 1979, 1981;

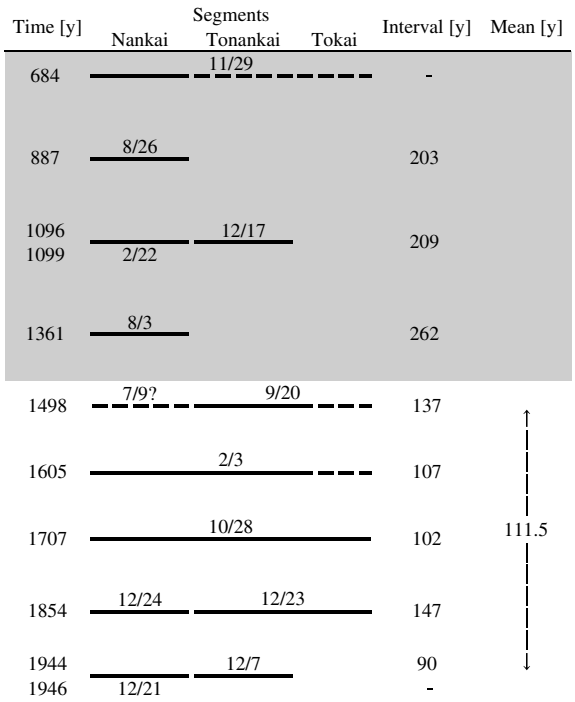

Figure 2. Occurrence times and source regions of historical great earthquakes along the Nankai trough. Data are from *Ando* [1999] for the events of 1361 and before, *Tsuji* [1999] for the 1498 Nankai earthquake, and *Earthquake Research Committee* [2001] for other events. Broken lines indicate less reliable data. Historical records may be incomplete before 1498 (shaded area). The mean recurrence interval was calculated only for events from 1498 to 1946.

Ruina, 1983; *Beeler et al*., 1994]. *Kuroki et al*. [2004] simulated recurring LSSEs beneath Lake Hamana at intervals of about 60 years before the cyclic Tokai earthquakes of M_w 8.3 that occur at intervals of about 450−500 years by introducing a zone of larger L than that in other area within the seismogenic region. However, because they used the overshooting method employed by *Tse and Rice* [1986] in order to save the calculation time for the coseismic rupturing process, unrealistic stresses were produced in shallow and deep parts of seismogenic zone just after (the occurrence of) a Tokai earthquake in their model, which effects the result of LSSE simulation. On the other hand, *Hirose et al*. [2009] simulated recurring LSSEs beneath Lake Hamana at intervals of about 30−40 years before the cyclic Tokai earthquakes of M_w 8.3−8.4 that occur at intervals of about 300−400 years by introducing heterogeneous friction parameters on the plate interface parallel to the trench axis and without the overshooting method. However, their study area did not include the Tonankai and Nankai segments, which implies an unrealistic assumption of a constant slip at the rate of plate convergence for those segments where the plate boundary is locked actually [*Kobayashi et al*., 2006; *Ozawa and Sagiya*, 2008]. Therefore, their simulation results may be affected by overestimated stress caused by assuming a constant slip in the Tonankai and Nankai segments.

[6] Our principal objective is to simulate in the 3-D model that the Tokai segment did not rupture and LSSEs have recurred beneath Lake Hamana. To ensure that our study took into account regional effects at the plate boundary and avoided the unrealistic assumptions of *Hirose et al*. [2009], we chose an area that extends from the Tokai region to western Shikoku. We simulated the 1944 Tonankai earthquake without rupture of the Tokai segment by applying mainly large values of L (similar to those of *Hori* [2006] and *Hirose et al*. [2009]) to take into consideration ridges subducted beneath the Tokai district, and we investigated the effect of L on the rupture resistance for the Tokai segment. In addition, we also examined the case of large σ in subducted ridges to arrest the rupture of the Tokai segment. We also attempted to simulate recurring LSSEs in the Tokai region by applying locally small effective normal stress beneath Lake Hamana, where dehydration of the Philippine Sea slab is assumed to be intense [*Hirose et al*., 2008b; *Matsubara et al*., 2008]. In addition, we investigated the effects of L in subducted ridges on LSSEs; L and σ beneath Lake Hamana on LSSEs; and different friction law (slip law [*Beeler et al*., [1994]).

2. Model and Modeling Parameters

2.1. Model

[7] Our model is a system of two plates in a uniform elastic medium filling a three-dimensional half space. The steady relative motion between the two plates at depth generates dislocations on the shallow part of the plate interface, which we approximated by a set of three-dimensional 7292 triangular cells with dip and strike dimensions of about 7 km to a depth of 50 km to represent the curvature of the plate interface (Figure 3a). For simplicity, we considered only the component of fault movement in the direction of relative plate motion and the variation of static shear stress on the fault only in this direction. Shear stress τ_i at the center of the ith cell induced by the slip u_j at the jth cell at time t can be expressed as

$$\tau_i(t) = \sum_{j=1}^{N} K_{ij}\left(V_j^{pl}t - u_j(t)\right) - \frac{G}{2\beta}\frac{\mathrm{d}u_i(t)}{\mathrm{d}t}, \qquad (1)$$

where K_{ij} is the static shear stress at the center of the ith cell caused by a unit of slip on the jth cell, and V_j^{pl}, G, and β are plate convergence rate at the jth cell, rigidity, and shear-wave speed, respectively. Values of K_{ij} are simply obtained by using a stress formula of dislocation expressed in terms of Green's function in a uniform elastic medium occupying a half space [*Mura*, 1987; *Kuroki et al*., 2002; H. Ito, personal communication, 2005]. The second term on the right-hand side of equation (1) represents shear-stress reduction during high-speed slip, and was introduced by *Rice* [1993] to approximate quasi-dynamic slip behavior during earthquakes. For elastic moduli, we used G = 30 GPa, a Poisson's ratio of 0.25, and β = 3.75 km/s.

[8] We assumed that the shear stress on the fault obeys a RSF law derived from laboratory experiments. Among the many versions of friction laws, we used here the composite law [*Kato and Tullis*, 2001] which applies a "slip law" in the high slip-velocity range and a "slowness law" in the low slip-velocity range, which fits laboratory data better than some other versions [*Dieterich*, 1979; *Beeler et al*., 1994].

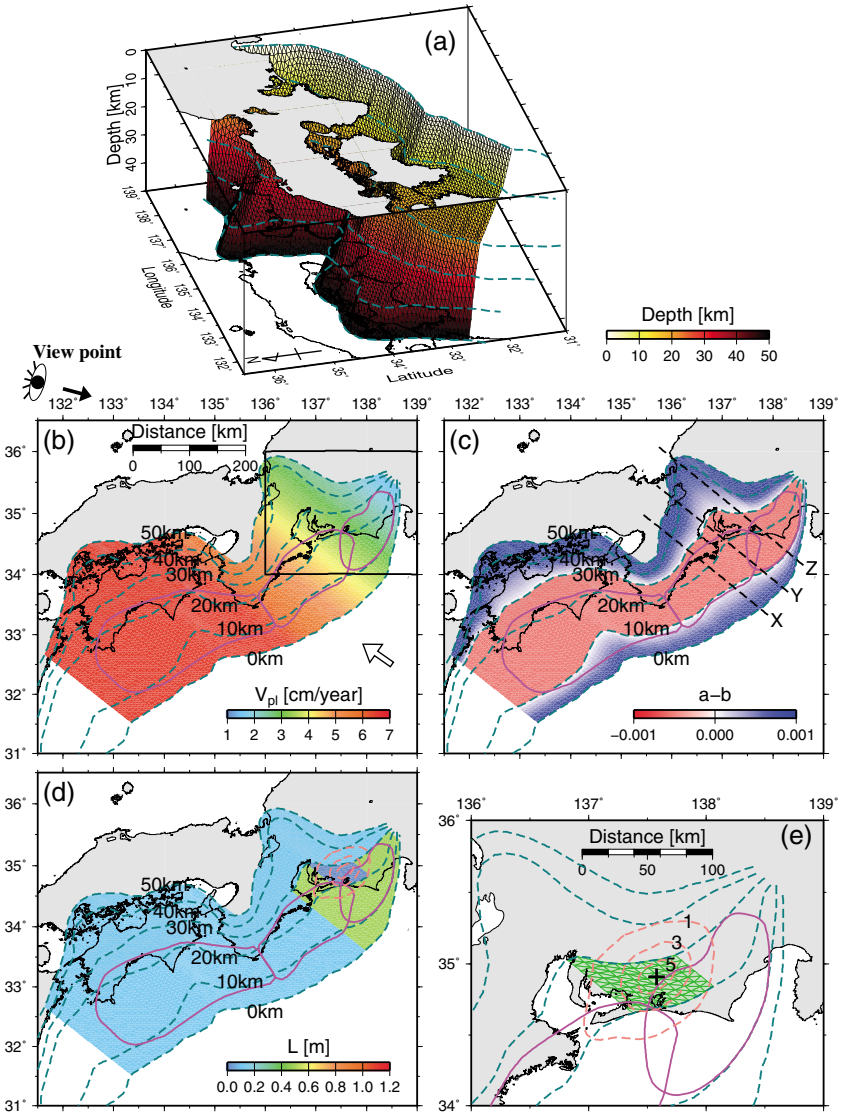

Figure 3. (a) Three-dimensional computational cells used in simulations. Map-view of (b) plate convergence rate V_{pl} [*Heki and Miyazaki*, 2001], (c) friction parameter ($a - b$), (d) characteristic displacement L, and (e) the area in Tokai region where high pore pressure was assumed (green shaded cells). The rectangle in Figure 3b shows the area of Figure 3e. Broken pink lines in Figure 3d and 3e are contours of the Tokai slow slip rate (1, 3, 5 cm/yr) on the plate interface during 2001–2005 [*Geographical Survey Institute*, 2007]. Broken lines X to Z in Figure 3c are locations of cross sections shown in Figure 4 and the cross in Figure 3e refers to the location of data shown in Figures 8, 11, and 17. Depth contours to the top of the subducting Philippine Sea plate, the postulated source areas, and the direction of movement of the Philippine Sea plates relative to the land plate are as shown in Figure 1.

According to this friction law, the frictional stress on the ith cell can be described as follows:

$$\frac{\tau_i(t)}{\sigma_i} = \mu_i(t) = \mu_0 + \Theta_i(t) + a_i \ln\left(\frac{V_i(t)}{V_0}\right), \tag{2}$$

$$\frac{d\Theta_i(t)}{dt} = \frac{V_0}{L_i} b_i \exp\left[-\left(\frac{V_i(t)}{V_c} + \frac{\Theta_i(t)}{b_i}\right)\right] - \frac{V_i(t)}{L_i}\left(\Theta_i(t) + b_i \ln\frac{V_i(t)}{V_0}\right), \tag{3}$$

where τ_i, σ_i, μ_i, and Θ_i are frictional stress, effective normal stress, frictional coefficient, and the state variable [*Nakatani*, 2001], respectively, of the ith cell. For simplicity, the effective normal stress is assumed to be constant in time. V_0 is an arbitrarily chosen reference velocity, which is set at 1.0×10^{-6} m/s. Parameter μ_0 is the steady state frictional coefficient at slip rate $V = V_0$ and is set at 0.6. V_c is a cutoff velocity for the composite law and is set at 1.0×10^{-8} m/s in accordance with *Kato and Tullis* [2001]. Parameters a, b, and L are constant frictional parameters that control sliding behavior on the fault. When $a - b < 0$ (velocity weakening), an unstable slip may occur because the strength decreases as the slip velocity increases. On the other hand, when $a - b > 0$ (velocity strengthening), unstable slip does not occur unless driven by a strong stress perturbation. Assuming

Table 1. Parameters Used Beneath Lake Hamana (LH), in Areas of Subducting Ridges, and in Other Regions for 19 Simulation Cases: Effective Normal Stress, Characteristic Displacement L, and Frictional Parameter ($a - b$) at Depths of 10−30 km[a]

	Effective Normal Stress (MPa)			L (m)				l_c (km)			Recurrence Interval (years)		
Case	Lake Hamana	Ridge	Other	LH	Ridge	Other	($a - b$) at Depths of 10–30 km	LH	Ridge	Other	Slow Slip	Earthquake	Rupture (R) or Not Rupture (N) of the Tokai Segment
1	30	100	100	0.0165	0.13	0.13	−0.00055	30	71	71	-	114	R
2	30	100	100	0.0165	0.2	0.13	−0.00055	30	109	71	-	113	R
3	30	100	100	0.0165	0.3	0.13	−0.00055	30	164	71	12–18	113/112	R/N
4	30	100	100	0.0165	0.4	0.13	−0.00055	30	218	71	11–14	114/111	R/N
5	30	100	100	0.0165	0.5	0.13	−0.00055	30	273	71	9–12	115/112	R/N
6	30	100	100	0.0165	0.6	0.13	−0.00055	30	327	71	9–12	115/112	R/N
7	30	100	100	0.0165	0.7	0.13	−0.00055	30	382	71	9–12	115/110	R/N
8	30	100	100	0.0165	0.8	0.13	−0.00055	30	436	71	9–12	115/109	R/N
9	20	100	100	0.0110	0.5	0.13	−0.00055	30	273	71	6–8	115/112	R/N
10	40	100	100	0.0220	0.5	0.13	−0.00055	30	273	71	13–18	115/112	R/N
11	50	100	100	0.0275	0.5	0.13	−0.00055	30	273	71	17–20	115/112	R/N
12	60	100	100	0.0330	0.5	0.13	−0.00055	30	273	71	22–25	115/112	R/N
13	70	100	100	0.0385	0.5	0.13	−0.00055	30	273	71	27	115/112	R/N
14	80	100	100	0.0440	0.5	0.13	−0.00055	30	273	71	-	115/112	R/N
15	30	100	100	0.0110	0.13	0.13	−0.00055	20	71	71	13–15	114	R
16	30	100	100	0.0200	0.5	0.13	−0.00055	36	273	71	10–14	115/112	R/N
17	100	100	100	0.1300	0.5	0.13	−0.00055	71	273	71	-	115/112	R/N
18	30	200	100	0.0165	0.13	0.13	−0.00055	30	35	71	17–19	114/111	R/N
19	30	100	100	0.0125	0.5	0.08	−0.00066	19	227	36	11–12	115/110	R/N

[a]Simulated recurrence intervals of slow slip events and earthquakes are also shown. Note that the frictional law used in simulations was the composite law for cases 1–18 and the slip law for case 19. See text for description of l_c.

that equilibrium between shear stress and frictional stress remains quasi-static, we numerically solved equations (1)–(3) simultaneously by the fifth-order Runge-Kutta method with an adaptive step-size control [*Press et al*., 1992]. The initial condition was $\mu_i(0) = \mu_0 + (a_i - b_i)\ln(V_i(0)/V_0)$ and $V_i(0)$ = 0.1 cm/y (3.1688×10^{-11} m/s) for all cells. Note that because we cannot apply the periodical solution [e.g., *Rice*, 1993] due to the three-dimensional cells which represent the curvature of the plate interface, equation (1) assumes that a constant slip at the plate convergence rate occurs outside the study area.

2.2. Parameter Setting

[9] We used the configuration of the Philippine Sea plate estimated by *Hirose et al*. [2008b] (see depth contours for Philippine Sea plate interface in Figures 1 and 3). *Hirose et al*. [2008b] revealed the widespread existence of layers with low V_s and high V_p/V_s ratio in southwestern Japan by using the double-difference tomography method of *Zhang and Thurber* [2003]. By combining the results of tomography and seismic refraction surveys, and considering the location of the slab Moho as delineated by receiver function analyses, *Hirose et al*. [2008b] interpreted the top of these layers to

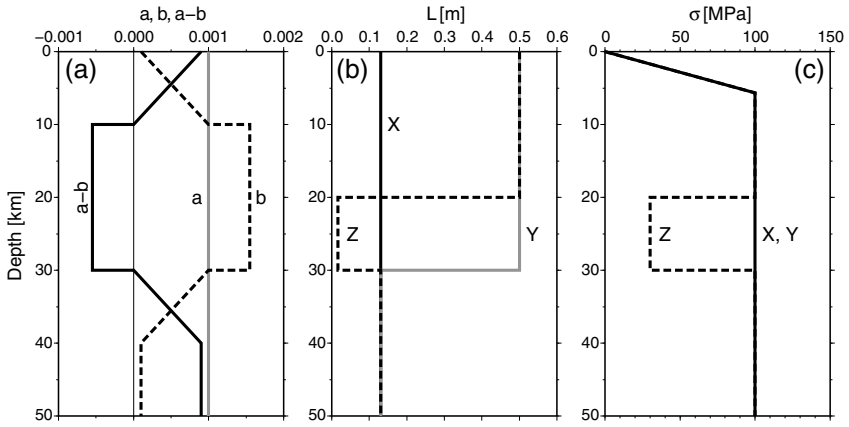

Figure 4. Depth distribution along lines X, Y, and Z of (a) friction parameters (a, b, and $a - b$), (b) characteristic displacement (L), and (c) effective normal stress (σ). Locations of lines X to Z are shown in Figure 3c.

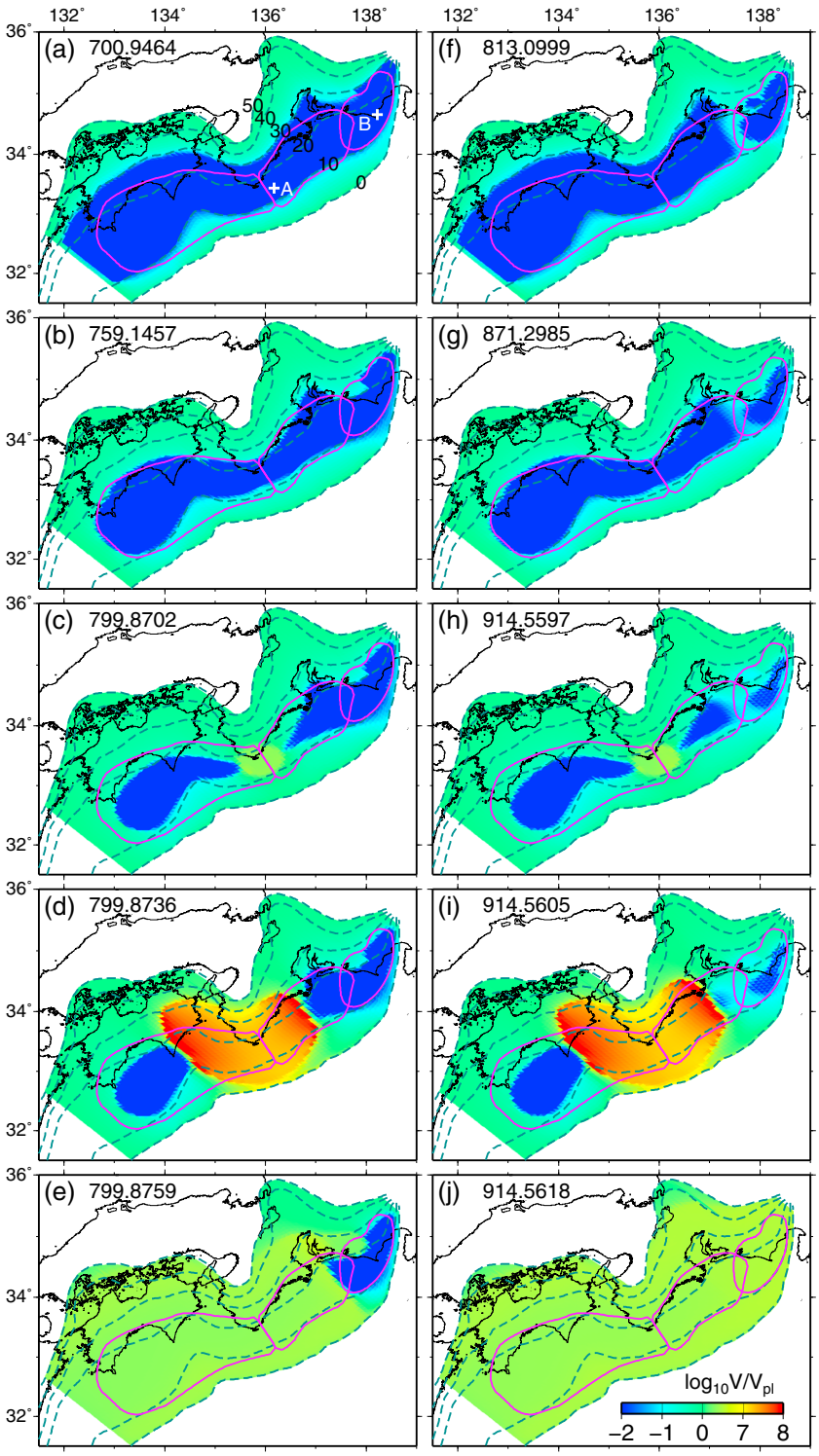

Figure 5

represent the upper surface of the Philippine Sea slab in southwestern Japan. The depth of the plate boundary estimated by *Hirose et al*. [2008b] is generally 5–7 km shallower than that based on the upper envelope of the hypocenters, which has previously been interpreted to represent the plate boundary [e.g., *Noguchi*, 1996; *Miyoshi and Ishibashi*, 2004].

[10] Our simulation area (Figure 3) included the postulated source regions of Tokai, Tonankai, and Nankai earthquakes [*Central Disaster Management Council*, 2001; *Earthquake Research Committee*, 2001]. For simplicity, we considered that frictional parameters a and b depend only on depth and that the seismogenic zones for which $(a - b)$ is negative are within the depth ranging from 10 to 30 km [cf. *Blanpied*

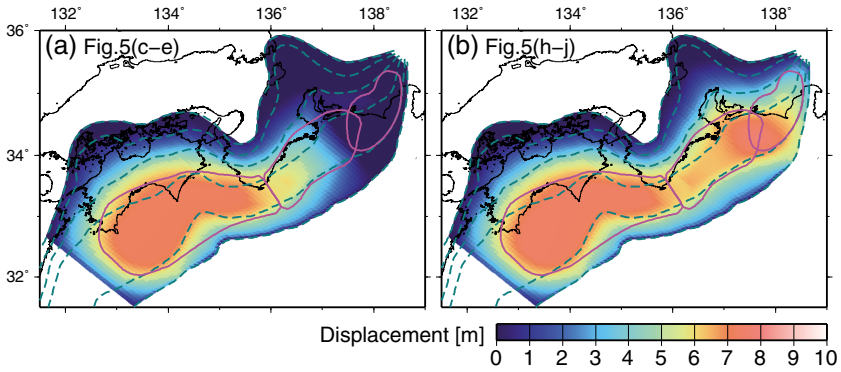

Figure 6. The spatial distribution of slip displacement on the plate interface for case 5 during a great earthquake: (a) without rupture of the Tokai segment from Figures 5c–5e and (b) with rupture of the Tokai segment from Figures 5h–5j. Depth contours to the top of the subducting Philippine Sea plate and the postulated source areas are as shown in Figure 1.

et al., 1991; *Hyndman et al*., 1995] (Table 1, Figures 3c and 4a). We applied these values because the value similar to the minimum value of $(a - b)$, -5.5×10^{-4}, are suggested in some models [e.g., *Kato and Tullis*, 2003; *Kuroki et al*., 2004]. Note that deep parts of seismogenic regions in this study (Figures 3c, 6, 13, and 15) are different from those that are postulated by *Central Disaster Management Council* [2001] and *Earthquake Research Committee* [2001] (areas enclosed by purple lines in Figure 3c) using the plate boundary data based on the upper envelope of hypocenters [e.g., *Noguchi*, 1996] and an assumption that the seismogenic zones are within the depth ranging from 10 to 30 km [cf. *Hyndman et al*., 1995]. We plotted postulated source regions in our figures to show rough position of three earthquakes. The plate convergence rate and the value of $(a - b)\sigma$ in the seismogenic zone control the recurrence interval of great interplate earthquakes. We chose values of $(a - b)$ such that the simulated recurrence interval was close to the historical average recurrence interval of 110 years for great earthquakes along the Nankai trough (Figure 2), assuming the plate convergence rates of *Heki and Miyazaki* [2001] and an effective normal stress of 100 MPa [*Rice*, 1992] except for beneath Lake Hamana where LSSEs have occurred. The plate convergence rate we used along the Nankai trough was 6.5 cm/y in the western part of the study area, decreasing eastward from the Kii Peninsula to 1.5 cm/y in the eastern part of the study area (Figure 3b) [*Heki and Miyazaki*, 2001]. We assumed the direction of plate convergence to be N55°W throughout the study area, which is an average of the values of *Heki and Miyazaki* [2001], and we did not change it during the simulation.

[11] When hydrated minerals in oceanic crust are subducted to great depth, they undergo phase transformations, liberating large amounts of water [e.g., *Hacker et al*., 2003]. Dehydration reactions at the plate boundary increase pore pressures when the released fluids are trapped by, for example, low permeability, which in turn reduce the effective normal stress and weaken coupling at the plate boundary. We adopted the excess pore pressure model of *Rice* [1992], as shown in Figure 4c. *Hirose et al*. [2008b] and *Matsubara et al*. [2008] showed that the regions where LSSEs occur coincide with areas of high V_p/V_s ratio, and attributed this to the presence of water produced by dehydration reactions. Therefore, we believe that the dehydration process is especially active in the subducting slab beneath Lake Hamana [*Hirose et al*., 2008b; *Matsubara et al*., 2008], so we used smaller effective normal stresses (20−80 MPa) at the plate interface beneath Lake Hamana than the 100 MPa we used elsewhere (Table 1, Figure 4c).

[12] L has been estimated to be a few micrometers in laboratory experiments [e.g., *Dieterich*, 1979], but we adopted much larger values (Table 1, Figures 3d and 4b) because the characteristic displacements in real fault systems are of the order of a few centimeters to a few meters [e.g., *Guatteri et al*., 2001]. The large L value is also required due to the limitation of calculation time associated with the critical cell size in the later description and the number of

Figure 5. Snapshots of the spatial distribution of slip velocity normalized by plate convergence rates [*Heki and Miyazaki*, 2001] on the plate interface for simulation case 5 using the composite law. The cold and warm colors indicate locking and sliding state on the plate interface, respectively. The number at the top of each panel is elapsed time (years) from commencement of the simulation. Depth contours to the top of the subducting Philippine Sea plate and the postulated source areas are as shown in Figure 1. (a) The most of seismogenic zone recovers locking state about 13 years after a great earthquake which ruptures whole regions. (b) Locked regions become smaller with time. (c) A pre-slip area extends off the Kii Peninsula, and a great earthquake rupture initiates. (d) The ruptures spread bilaterally from the epicenter. (e) The Tokai segment remains locking while the ruptured area shows an after-slip. (f) The most of seismogenic zone recovers locking state about 13 years after a great earthquake except for regions between the Tokai and Tonankai segments. (g) Locked regions become smaller with time. (h) A pre-slip area extends off the Kii Peninsula, and a great earthquake rupture initiates. (i) The ruptures spread bilaterally from the epicenter. (j) The whole regions including the Tokai segment are ruptured. And the state on the plate interface comes back to Figure 5a.

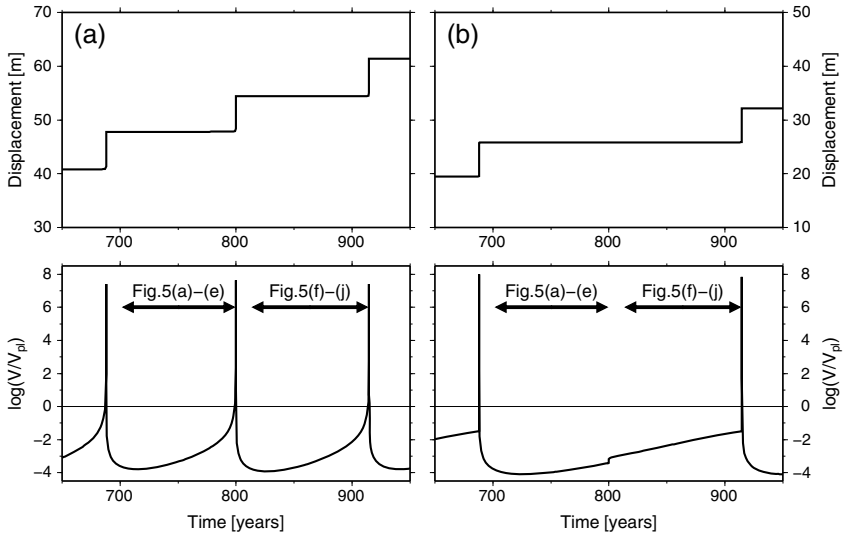

Figure 7. Time evolution of (top) cumulative displacement and (bottom) and slip velocity normalized by plate convergence rate for case 5 at locations marked by white crosses in Figure 5a. (a) White cross A, (b) white cross B.

meshes. Table 1 shows the parameters we used for each simulation in this study. Cases 1–8 show the relationship between unbroken area of the Tokai segment and L in the range 0.13−0.8 m for ridges subducted beneath the Tokai region. Regions where L is large can behave as barriers against rupture propagation because the energy required for rupture increases in proportion to L [*Rubin and Ampuero*, 2005]. Therefore, in our simulations, we assigned large values of L to the regions near subducted ridges in the Tokai segment like *Hori* [2006] and *Hirose et al*. [2009]. Cases 5, 9–14 show the response of LSSEs to the change of effective normal stress σ and L beneath Lake Hamana, where we assume h^* (see below) is constant. Case 15 shows LSSEs occur even if L in areas of subducted ridges is not relatively large. Case 16 shows that the change of L affects the amplitudes of LSSEs in comparison with case 5. Case 17 shows that LSSEs do not occur when σ and L are not locally set low. Case 18 shows that an increased σ instead of large L in subducted ridges can also behave as barriers against rupture propagation (similar to those of *Honkura et al*. [1999], *Hori* [2006], and *Yang et al*.[2012]). Finally, case 19 shows the simulation result using the slip law instead of the composite law.

[13] *Rice* [1993] derived the critical cell size h^* ($= GL/(b-a)\sigma$) required to satisfy the continuum approximation and demonstrated that the computation cell size h must be smaller than h^*. For the ith cell, h/h^* is given theoretically by $(b_i - a_i)\sigma_i/L_iK_{ii}$ [*Hori et al*., 2004]. For our simulations, h/h^* was always smaller than 0.225 (the maximum value in the area of high pore pressure beneath Lake Hamana); elsewhere, except for the areas of subducted ridges, it was always smaller than 0.121. *Liu and Rice* [2005] showed that for values of h/h^* between 0.25 and 0.125, there was minimal effect on simulated slip displacements and slip rates. Therefore, we believe that the resolution of our numerical model was sufficient to evaluate the occurrence patterns of great earthquakes and LSSEs in the Tokai region because the maximum value of h/h^* is 0.225.

3. Results

3.1. Simulation of Great Earthquakes Along the Nankai Trough

[14] We performed 19 numerical simulations in total, and parameters for them are listed in Table 1 (refer also to Figures 3 and 4). All cases showed that great earthquake ruptures initiate off the Kii Peninsula and spread bilaterally from there. *Takayama et al*. [2008] researched the effect of three-dimensional plate boundary configuration on initiation points of great earthquakes along the Nankai trough. The narrower the width of the seismogenic zone along dip direction becomes, the larger the stress concentration for the seismogenic zone is. Thus, the earthquake ruptures initiate off the Kii Peninsula where the seismogenic zone is narrower than other region. Note that the stress concentration is not large at the Tokai region due to the lowest plate convergence rate although the seismogenic zone at that region is the narrowest.

[15] The simulated ruptures do not always propagate as far as the Tokai segment, as was the case for the 1944 Tonankai and 1946 Nankai earthquakes, except for cases 1, 2, and 15 where relatively small L is applied to the region of subducted ridges and we expect less effect of barriers against rupture propagation [*Rubin and Ampuero*, 2005] (see section 4.1). For case 5 simulation, as an example, a great earthquake that ruptures both the Tonankai and Nankai segments occurs about every 112−115 years, but the rupture propagates into the Tokai segment for only every second earthquake (i.e., about every 220 years; Figures 5 to 7). According to our case 5 simulation, the moment magnitude M_w of a great earthquake is 8.8 when the entire region along Nankai trough ruptures, and 8.7 when only the Nankai and Tonankai segments rupture. Note that M_w was estimated from the relationship $\log M_0 = 1.5M_w + 9.1$ [*Kanamori*, 1977], where M_0 [Nm] is obtained from the slip distribution of the coseismic zone, which is defined here as the area for which slip velocity is higher than 0.1 m/s.

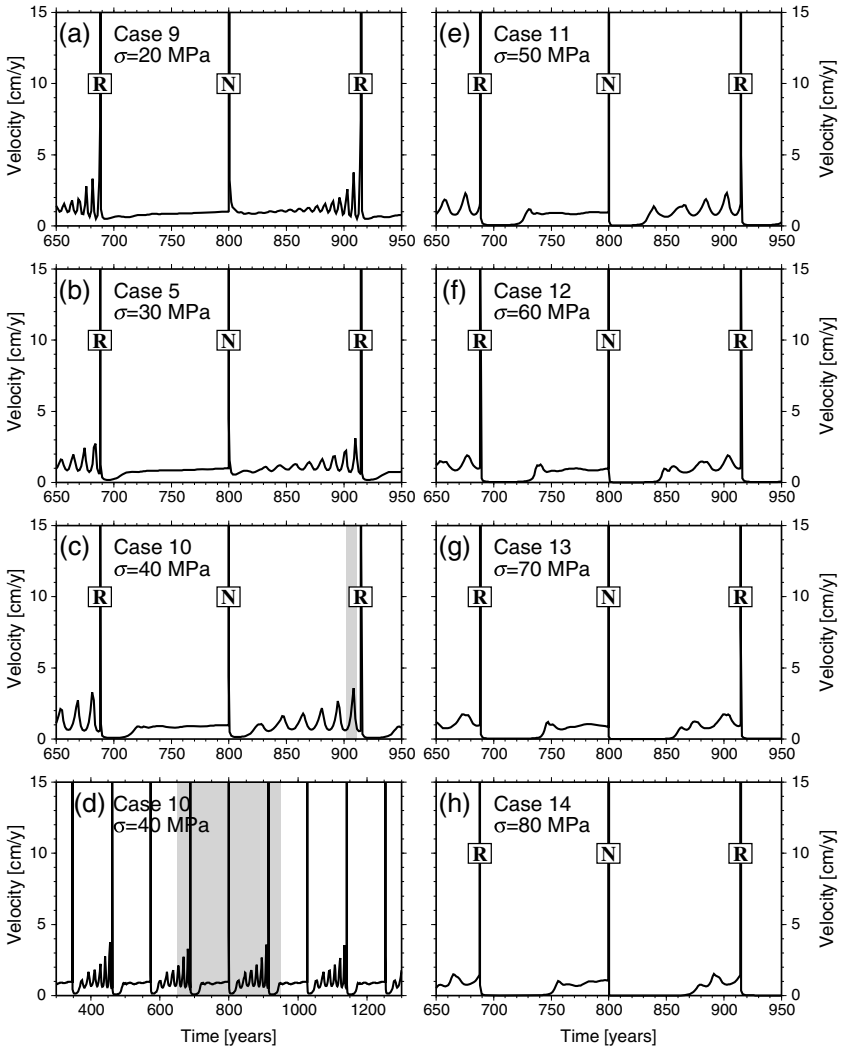

Figure 8. (a–h) Time evolution of slip velocity for cases 5, 9–14 at the location of the cross in Figure 3e. The shaded period in Figure 8d is enlarged in Figure 8c. R and N denote the occurrence of great earthquakes during which the Tokai segment is ruptured and not ruptured, respectively. The shaded interval in Figure 8c refers to data presented in Figure 10.

[16] The simulated area of the case 5 for Tokai region without rupture (shown in Figures 5e and 6a) is approximately equal to the area where no slip was observed during the 1944 Tonankai earthquake [*Ichinose et al*., 2003; *Kikuchi et al*., 2003] and also agrees with the postulated source area of the next Tokai earthquake [*Central Disaster Management Council*, 2001].

[17] Because in our model the Tonankai and Nankai earthquakes always occur at the same time, the simulated results are inconsistent with historical records, which show that earthquakes in these regions have not always occurred at the same time (Figure 2). However, because the interval between them is generally small (from days to about 2 years) compared to the recurrence interval (about 110 years), this inconsistency has little effect on the simulated occurrence patterns of the Tokai earthquake or LSSEs.

3.2. Simulation of the Slow Slip in the Tokai Region

[18] The time evolution of LSSE slip rates beneath Lake Hamana for cases 5, 9–14 (Figure 8) clearly shows that the

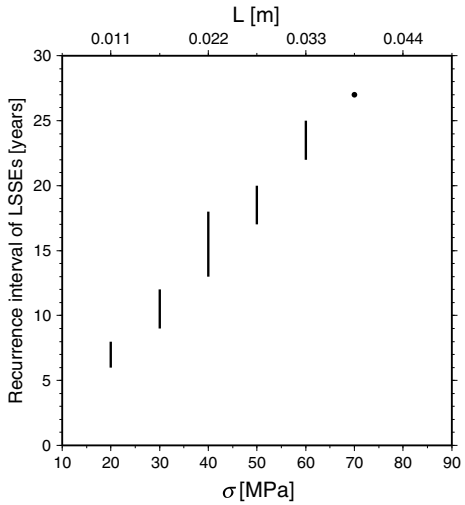

Figure 9. Recurrence periods of modeled LSSEs as a function of the assigned effective normal stress σ and characteristic displacement *L* beneath Lake Hamana.

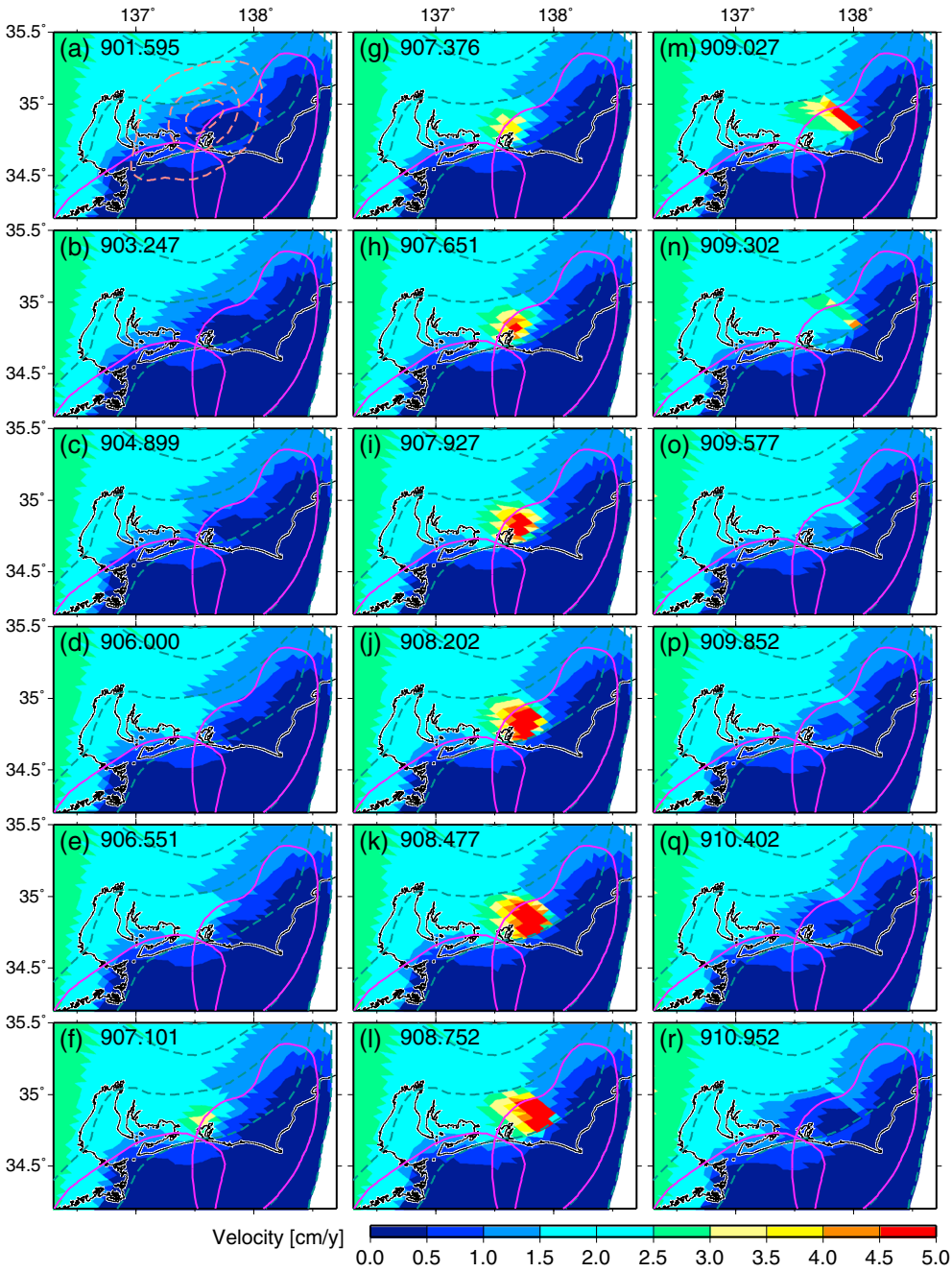

Figure 10. (a–r) Snapshots of the spatial distribution of slip velocities on the plate interface for case 10 in the shaded interval in Figure 8c. The cold and warm colors indicate locking and sliding state on the plate interface, respectively. The number at the top of each panel is elapsed time (years) from the start of the simulation. Broken pink lines in Figure 10a are contours of the Tokai slow slip rate (1, 3, 5 cm/yr) on the plate interface during 2001–2005 [*Geographical Survey Institute*, 2007]. Depth contours to the top of the subducting Philippine Sea plate and the postulated source areas are as shown in Figure 1. In Figures 10a and 10b, the most of seismogenic zone remains locking. In Figures 10c–10n, stable sliding on the plate interface at depth gradually invaded the shallow locked region. Then locked regions become smaller with time and LSSE occurs. In Figures 10o–10r, locked regions become larger with time due to the healing process.

amplitudes of simulated LSSEs increase after earthquakes during which the Tokai segment does not rupture, whereas they are negligible after that segment has ruptured. After a great earthquake without rupture of the Tokai segment, LSSEs with a certain level of amplitude begin after an interval that is positively correlated with normal stress σ beneath Lake Hamana.

[19] Our simulations clearly show that as the effective normal stress was increased, the recurrence interval of LSSEs also increased (Table 1, Figures 8 and 9). There were

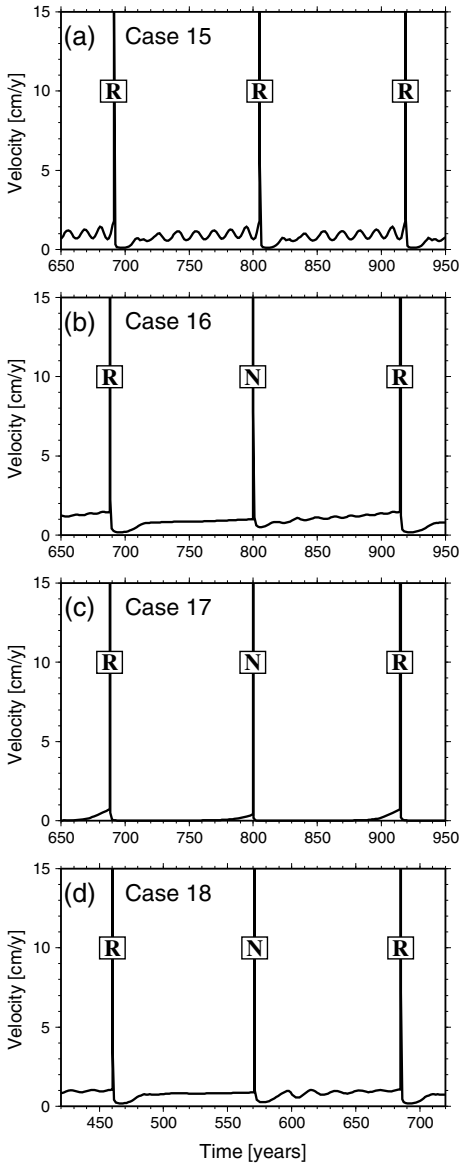

Figure 11. Time evolution of slip velocity for (a) case 15, (b) case 16, (c) case 17, and (d) case 18 at the location marked by a cross in Figure 3e. R and N denote the occurrence of great earthquakes during which the Tokai segment is ruptured and not ruptured, respectively.

no recurring LSSEs when σ was greater than or equal to 80 MPa (case 14 in Table 1). The value of $(a - b)\sigma$ in the seismogenic zone controls the stress drop of great interplate earthquakes. The dependency of the length of the period of LSSEs on normal stress can be explained by the need for sufficient time to accumulate the shear stress required to produce LSSEs, and that the amount of time is dependent on the amount of stress drop. Furthermore, for cases 5, 9−12 (Table 1, Figures 8a–8f), the intervals between LSSEs became gradually shorter as time passed because a constant slip at the plate interface at depth gradually invaded the shallow locked region and accelerated the rate of stress accumulation in the area of slow slip. The LSSEs gradually increase in amplitude up to the time of the next great earthquake (Figure 8). The increase of the LSSE velocity in our simulation is consistent with the observation that a magnitude of the last Tokai LSSE during 2001−2005 was larger than that of the LSSE during 1988−1990 [*National Research Institute for Earth Science and Disaster Prevention*, 2004; *Kobayashi and Yoshida*, 2004].

[20] Figure 10 shows the spatial distribution of the simulated slip rates of LSSEs beneath Lake Hamana for case 10. The simulated slip rate distribution is consistent with the observed distribution measured from GPS data for the Tokai SSE during 2001−2005 [*Geographical Survey Institute*, 2007]. Simulated LSSE whose maximum velocity is ~5 cm/yr (Figure 10) is also consistent with the observed velocity estimated from GPS inversion by *Geographical Survey Institute* [2007]. On the other hand, *Miyazaki et al*. [2006] estimated it at ~15 cm/yr from GPS inversion. We consider that one of the causes of this discrepancy is a difference in configuration of the Philippine Sea plate used in each study because the plate configuration that *Miyazaki et al*. [2006] used is deeper than those that we and *Geographical Survey Institute* [2007] used. The moment rate of the Tokai slow slip during 2001−2005 was estimated to be 5.5×10^{11} Nm/s [*Geographical Survey Institute*, 2007]. If a slow slip area is taken to be an area where $V \geq V_{pl}$, the moment rate we estimated for a simulated LSSE was 10^{10}−10^{11} Nm/s, which agrees well with the estimate of the *Geographical Survey Institute* [2007].

[21] We used case 15 (Table 1) to investigate the effect of large L in areas of subducted ridges on LSSEs. In case 15, we did not assign a large L in areas of subducted ridges, but still simulated recurring LSSEs (Figure 11a). Because σ and L beneath Lake Hamana were locally small, even for an L of 0.13 m in areas of subducted ridges (the same L value as that in the surrounding region), L for subducted ridges remained large enough to form a barrier to the growth of LSSEs into subducted ridges. However, in case 15, the Tokai segment ruptured every time the Tonankai segment ruptured, and always produced a great earthquake that ruptured along the entire Nankai trough. This result shows that large L in areas of subducted ridges is essential to avoid rupture of the Tokai segment during the 1944 Tonankai earthquake.

[22] Comparison of cases 5 and 16 shows that changes of L affect the amplitudes of LSSEs (Figures 8b and 11b). Increasing the value of L lowers the slip weakening rate and increases the frictional energy that resists sliding [*Rubin and Ampuero*, 2005], making unstable sliding difficult. Therefore, large values of L lower the amplitudes of slow slips. This sensitive relation between L and the amplitude of LSSEs may be used to estimate the value of L in a slow slip area, although we did not take into consideration the dependency of L on other parameters such as σ or $(a - b)$.

[23] Case 17, in which pore pressure and L beneath Lake Hamana are the same as those for other regions (other than ridge areas), can be used as a reference case that does not show recurring LSSEs (Figure 11c). Comparison of case 17 with other cases suggests that it is the locally elevated pore pressures and low values of L that are essential to the occurrence of slow slips. This is also supported by the evidence that the LSSEs occur with a recurrence interval of about 6 years beneath the Bungo channel [*Kobayashi and Yamamoto*, 2011], where the presence of water produced by dehydration reactions is also estimated from the

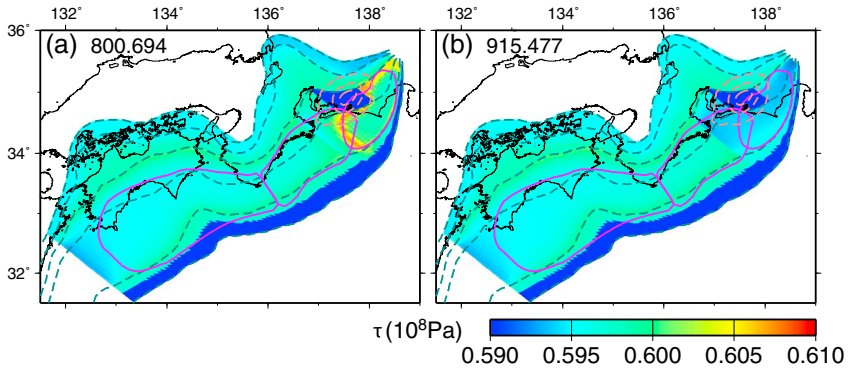

Figure 12. Snapshots of the spatial distribution of shear stress on the plate interface for case 5 immediately after a great earthquake: (a) without rupture of the Tokai segment and (b) with rupture of the Tokai segment. The number at the top of each panel is elapsed time (years) from the start of the simulation. Depth contours to the top of the subducting Philippine Sea plate and the postulated source areas are as shown in Figure 1.

distribution of high V_p/V_s ratio region obtained by tomography analysis [*Hirose et al*., 2008b].

[24] Figure 12 shows snapshots of the spatial distribution of shear stress on the plate interface just after a great earthquake when the Tokai segment is not ruptured (Figure 12a) and when it is ruptured (Figure 12b). Following the great earthquake without rupture of the Tokai segment, shear stress increased around the Tokai segment (Figure 12a), which caused repeated slow slips in the Tokai region. On the contrary, such a concentration of shear stress did not occur around the Tokai region when the Tokai segment ruptured during the earthquake (Figure 12b) and the amplitudes of Tokai LSSEs were very small, probably representing stable sliding at about 1 cm/yr (Figure 8). These modeling outcomes suggest that the distinctive LSSEs recently observed in the Tokai region are related to the lack of rupture of the Tokai segment during the 1944 Tonankai earthquake.

4. Discussion

4.1. Effect of Subducted Ridges

[25] The bathymetric map of the study area (Figure 1) shows parallel seafloor ridges on the Philippine Sea plate south of the Zenisu ridge off the Tokai region. *Kodaira et al*. [2004] showed that at least two ridges have been subducted under the Tokai region (Figure 1). The present bathymetry suggests that ridges on the Philippine Sea plate may have been regularly subducted beneath the Japanese arc since 15 Ma, when subduction of the Philippine Sea plate began [*Okino et al*., 1994]. Therefore, it is reasonable to assume the existence of subducted ridges deeper than the two identified by *Kodaira et al*. [2004].

[26] The plate boundary near the subducted ridges is not flat, but appears to be an undulating surface and rougher than other plate interface [*Kodaira et al*., 2004]. Laboratory experiments [*Dieterich*, 1979, 1981] show that the rougher the contact surface, the larger the characteristic displacement L. Note that we do not mean that surface roughness is comparable to L, but we assume it has some correlation with L. In addition, regions where L and/or σ are large can behave as barriers to rupture propagation because the energy required for rupture increases in proportion to L and/or σ [*Rubin and Ampuero*, 2005]. Therefore, first, we applied relatively large L to subducted ridges whose roughness is large. We extended the region with large L to depths of 0−30 km to take into consideration the possible existence of more subducted ridges, as discussed above. For L smaller than 0.4 m in areas of subducted ridges (cases 1−3 in Table 1), the simulations produced rupture on half of the Tokai segment, because the effect of the barrier was smaller and, instead of periodic LSSEs, stable sliding continued at a constant slip rate of about 1 cm/yr. In contrast, when L in areas of subducted ridges was larger than 0.6 m (cases 7 and 8), the simulation showed no rupture in the northeastern area of the Tonankai segment that ruptured during the 1944 Tonankai earthquake [*Baba and Cummins*, 2005] because the effect of the large-L barrier increased. Thus, L in areas of ridge subduction ranged from 0.4 to 0.6 m (cases 4–6), but note that the estimation of L depends on the assumed value of $(b - a)\sigma$. When only the two areas corresponding to the subducted ridges (see thick black lines in Figure 1) identified by *Kodaira et al*. [2004] were assigned large L (0.8 m), not placed in Table 1, only the southeastern half of the Tokai segment remained not ruptured because the effect of the large-L barrier was small, suggesting that there are more subducted ridges deeper beneath the Tokai region than those identified by *Kodaira et al*. [2004].

[27] So far we have considered mainly the effect of large L for subducted ridges to simulate rupture arrested in the Tokai segment. Next, we examined the effect of large σ for subducted ridges on the rupture arrest. *Honkura et al*. [1999] evaluated an additional effective normal stress due to subducted seamounts in the Tokai region as 100 MPa. Accordingly, we also applied an additional σ of 100 MPa (that is 200 MPa in total) to the same area of large L (green area) in Figure 3d. Note that we applied same L of 0.13 m in subducted ridges and other area to evaluate the effect of just σ (case 18 in Table 1). As a result of simulation, the rupture propagation stopped at the Tokai segment like cases of large L (cf., Figures 6 and 13) although the amplitudes of LSSEs became small (cf., Figures 8 and 11d). It would be possible to make the amplitudes of LSSEs large by tuning the parameter L beneath Lake Hamana in the similar manner in section 3.2 (cf., cases 5 and 16).

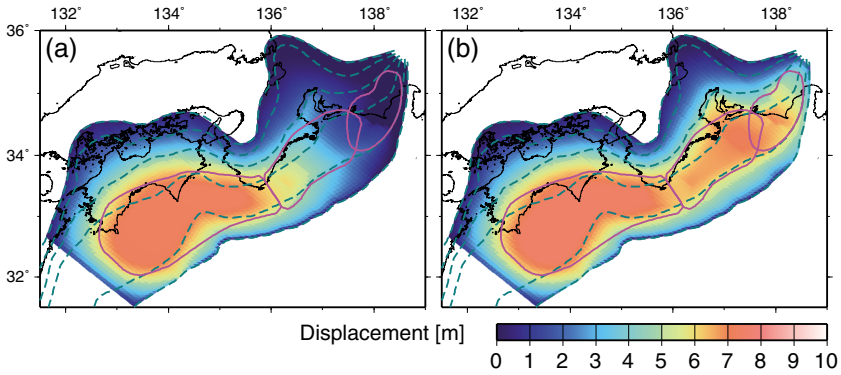

Figure 13. The spatial distribution of slip displacement on the plate interface during a great earthquake for case 18 applying an additional effective normal stress to subducted ridges: (a) without rupture of the Tokai segment and (b) with rupture of the Tokai segment. Depth contours to the top of the subducting Philippine Sea plate and earthquake source areas are as shown in Figure 1.

4.2. Comparison of This Study With Simulations by *Hirose et al.* [2009]

[28] In the modeling of *Hirose et al*. [2009], the last slow slip before the Tokai earthquake accelerated and spread widely, producing the earthquake. On the other hand, in the new model extended westward to Shikoku, the simulated Tokai slow slip did not grow into a large earthquake because the accumulation speed of shear stress off Kii Peninsula is faster than that in the Tokai region, thus an earthquake tends to initiate there [*Takayama et al*., 2008]. One reason why there was less acceleration of the Tokai slow slip in this study than in *Hirose et al*. [2009] is that by extending the model to the west, we have avoided unrealistic steady aseismic slip in the Tonankai segment, which was implicit in the modeling of *Hirose et al*. [2009], and which caused stress concentration in the Tokai segment. Another reason is that the large L that we introduced near subducted ridges to restrain the 1944 Tonankai earthquake from rupturing into the Tokai segment, also restrained the LSSE from expanding into the Tokai segment. When the length of a localized pre-slip region exceeds a critical length l_c [*Kato*, 2004], approximately equal to $GL/(b-a)\sigma = h^*$ [*Rice*, 1993], seismic slip occurs. Considering l_c (Table 1), the Tokai earthquake was not triggered by the LSSE because l_c (several hundred kilometers) near subducted ridges was much larger than the length of the slow slip area (several tens of kilometers in Figure 10), whereas the earthquake initiated off Kii Peninsula because l_c (~71 km) in that region was smaller than the along-dip dimension (at least ~80 km, see Figure 3c) of the seismogenic zone. It is noteworthy that when the Tokai earthquake occurred in our simulations, it was always preceded by a Tonankai earthquake.

4.3. Controls for Slow Slip Events

[29] We simulated recurring LSSEs in the Tokai region by applying low values for effective normal stress and L beneath Lake Hamana. Note that we applied large L to the subducted ridges in the Tokai region but small L to regions where the ridges are also expected to subduct beneath Lake Hamana where LSSEs have occurred. Because states of the plate boundary beneath Lake Hamana where dehydration process is especially active [*Hirose et al*., 2008b; *Matsubara et al*., 2008] are different from those of other regions, we consider that friction properties beneath Lake Hamana are also locally different from other regions. *Kato* [2004] showed that episodic aseismic slip events (slow earthquakes) may occur in a velocity-weakening patch whose size is approximately equal to or slightly smaller than the critical size (l_c) of earthquake nucleation. On the other hand, in our present model, l_c beneath Lake Hamana (~30 km, Table 1) is about half the length of the shaded green area in Figure 3e where the simulated Tokai LSSEs occurred, which apparently suggests that the relation of l_c to the size of the slow slip area of our model is inconsistent with the results of *Kato* [2004]. This may be explained by the difference of the frictional property around a velocity-weakening patch. In our model. a velocity-weakening patch is almost surrounded by velocity-weakening regions with large L and σ while in *Kato* [2004], it is surrounded by velocity-strengthening regions. The rate of stress accumulation from surrounded area to slow slip area becomes low when coupling rates are high (slip rates are low) in the surrounding area as our model (see Figure 10). The difference of stress accumulation rates in slow slip area between our model and *Kato*'s [2004] model is the reason why the slip speed remains slow even if the size of a velocity-weakening patch (the shaded green area in Figure 3e) is larger than l_c.

[30] As above mentioned, we found that it is necessary to assign low values of σ and L to the area beneath Lake Hamana in order to reproduce the recurring LSSEs. There are many studies on the mechanisms of reproducing the recurring LSSEs [e.g., *Liu and Rice*, 2007; *Rubin*, 2008; *Matsuzawa et al*., 2010]. For the case of partially locked plate interface, *Liu and Rice* [2007] and *Rubin* [2008] found that the parameter W/h^* determines the style of slip, where W is the width of the velocity-weakening zone between the locked zone and velocity-strengthening zone, and h^* is the critical cell size [*Rice*, 1993]. *Liu and Rice* [2007] showed that high pore pressure is required to explain observed recurrence intervals and slips of SSEs in the 2-D planar subduction model based on the RSF law with the slowness law [*Beeler et al*., 1994] for state evolution. *Rubin* [2008] pointed out that SSEs arise under small positive value of $(b-a)$ in combination with low effective normal stress in the 2-D planar subduction model similar to *Liu and Rice* [2007]. On the other hand, he also suggested that two mechanisms are

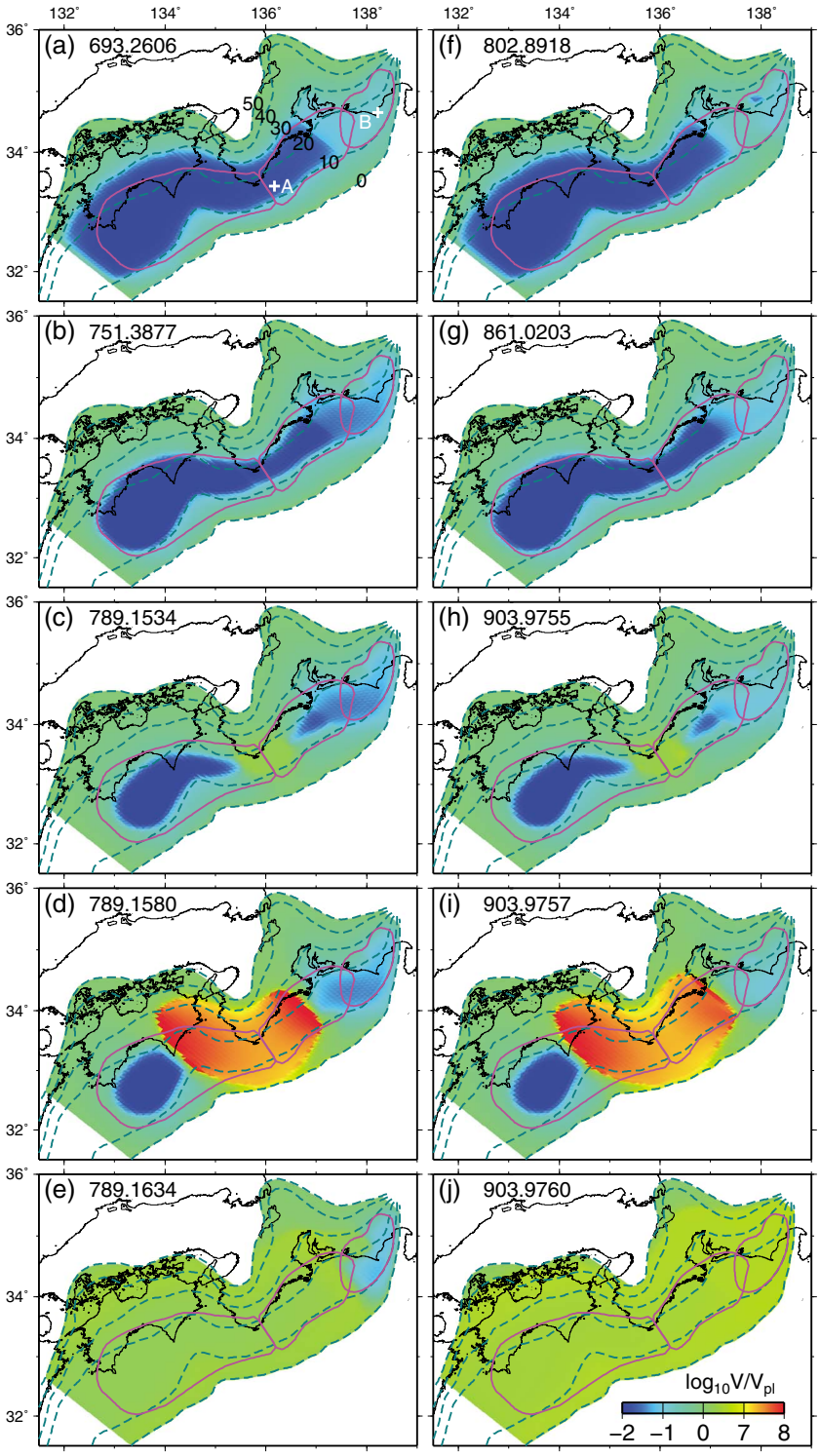

Figure 14

required for generating SSEs "stably" for the slip law which is relatively consistent with lab data rather than the slowness law: one is a transition of friction from velocity weakening to velocity strengthening at the appropriate slip speed, and the other is an inelastic dilatation of the fault zone coupled with pore pressure reduction and diffusive recovery. In our 3-D plate model, W beneath Lake Hamana has a range 40−70 km (the dip length of the shaded green area in Figure 3e) and the length in the strike direction is about 60 km. We used values of h^* in the range of 19–36 km to recur LSSEs (the same as l_c listed in LH in Table 1). Thus, W/h^* in the LSSEs regions has values ranging 1.11−3.68. These values

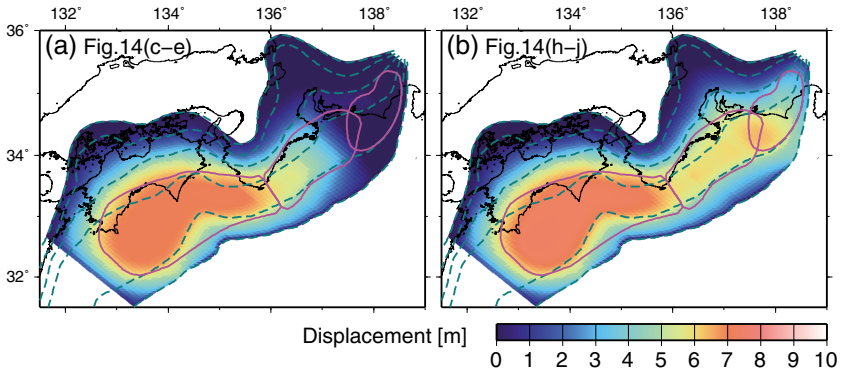

Figure 15. The spatial distribution of slip displacement on the plate interface for case 19 during a great earthquake: (a) without rupture of the Tokai segment from (Figure 14c–14e) and (b) with rupture of the Tokai segment from (Figure 14h–14j). Depth contours to the top of the subducting Philippine Sea plate and earthquake source areas are as shown in Figure 1.

are basically consistent with the slow slip condition suggested by *Rubin* [2008]. However, from our simulation results (e.g., compare case 1 with case 5 in Table 1), there are cases with and without recurring LSSEs even if W/h^* is the same value. Therefore, we think that although W/h^* may be an index for determining the style of slip in a 2-D planar subduction model with simple spatial distribution of parameters, complicated heterogeneous stress distribution and stress accumulation process are also related to make LSSEs to occur in a 3-D complex model. *Matsuzawa et al*. [2010] reproduced long- and short-term SSEs in the transition zone by adopting the RSF law with two cutoff velocities and assuming high pore fluid pressure in both of the 2-D and 3-D planar subduction models. Recurring SSEs tend to occur easily when steady state friction behaves as velocity weakening at low slip velocity and velocity strengthening at high slip velocity by incorporating two cutoff velocities, as pointed out by *Rubin* [2008]. However, it is unknown whether the friction law including two cutoff velocities is appropriate at depths where SSEs occur. As shown in the following section 4.4, we can also reproduce recurring LSSEs using the slip law instead of the composite law by assigning locally low values of σ and L without introducing a velocity-strengthening friction law at high slip velocity. Although there are differences in the friction laws and dimension of model space among these recent models, the term of a high pore pressure (low effective normal stress) may be the common keyword for generating SSEs. Therefore, it is necessary to estimate spatial distribution of pore fluid precisely [e.g., *Kato et al*., 2010] for the better modeling of LSSEs in the future.

4.4. Effect of Using Different Friction Laws

[31] For cases 1–18, we used the composite RSF law of *Kato and Tullis* [2001], which applies a "slip law" in the high slip-velocity range and a "slowness law" in the low slip-velocity range [*Beeler et al*., 1994]. *Hirose et al*. [2009] simulated the recurring Tokai slow slips by using the slip law. For case 19, we ran a simulation using the slip law instead of the composite law and also took into consideration the locally high pore pressures beneath Lake Hamana and the subducted ridges beneath the Tokai region.

[32] The simulation results for case 19 are very similar to those we generated using the composite law. That is, pre-slip occurred off Kii Peninsula, the rupture spread bilaterally from there, great earthquakes in Tonankai and Nankai segments occurred about every 110−115 years, and the rupture propagated to the Tokai segment only during every second great earthquake (Figures 14 to 17). It is noteworthy that we use the slip law and different values of friction parameters from these for the composite law in order to simulate the similar earthquake cycles (see case 19 in Table 1). For this model, the moment magnitude of the great earthquake when all three segments along the Nankai trough ruptured was 8.8; it was 8.7 when there was no rupture of the Tokai segment. Although the slip rates during the interseismic period

Figure 14. Snapshots of the spatial distribution of slip velocities normalized by plate convergence rates [*Heki and Miyazaki*, 2001] on the plate interface for case 19 using the slip law. The cold and warm colors indicate locking and sliding state on the plate interface, respectively. The number at the top of each panel is the elapse time (years) from the start of the simulation. Depth contours to the top of the subducting Philippine Sea plate and the postulated source areas are as shown in Figure 1. (a) The most of seismogenic zone recovers locking state about 14 years after a great earthquake which ruptures whole regions. (b) Locked regions become smaller with time. (c) A pre-slip area extends off the Kii Peninsula, and a great earthquake rupture initiates. (d) The ruptures spread bilaterally from the epicenter. (e) The Tokai segment remains locking while the ruptured area shows an after-slip. (f) The most of seismogenic zone recovers locking state about 14 years after a great earthquake except for regions between the Tokai and Tonankai segments. (g) Locked regions become smaller with time. (h) A pre-slip area extends off the Kii Peninsula, and a great earthquake rupture initiates. (i) The ruptures spread bilaterally from the epicenter. (j) The whole regions including the Tokai segment are ruptured. And the state on the plate interface comes back to Figure 14a.

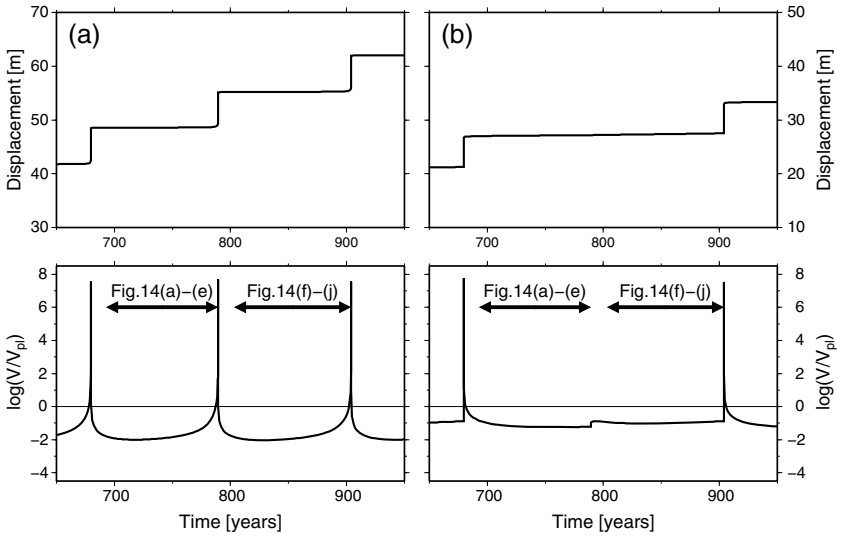

Figure 16. Time evolution of (top) cumulative displacement and (bottom) slip velocity normalized by plate convergence rate for case 19 at the locations marked by white crosses in Figure 14a. (a) White cross A, (b) white cross B.

differed for the composite and slip laws (see Figures 7 and 16), modeling with both laws simulated both the phenomena of recurring slow slips and the lack of rupture of the Tokai segment during every second great earthquake. Therefore, there was little difference in the simulation outcomes achieved using these two friction laws.

4.5. Problems to be Addressed in Future Studies

[33] Taking into consideration the results of *Hyndman et al*. [1995], we assumed in this study that the frictional parameter ($a - b$) depends only on depth [*Hirose et al*., 2008b] and does not change along the axis of the Nankai trough. However, *Hirose et al*. [2008a] suggested that the spatial distribution of temperature on the Philippine Sea slab, which controls the value of ($a - b$), does not necessarily mirror the iso-depth contours of the top of the slab. Therefore, future studies should include variation of ($a - b$) along the trough axis.

[34] In our model, great earthquakes along the Nankai trough always initiate off Kii Peninsula and the ruptures then propagate bilaterally; that is, the Tonankai and Nankai segments always rupture at the same time. Furthermore, the Tokai segment does not rupture in isolation, but it does rupture every second time the Tonankai segment ruptures. These simulated results are not completely consistent with the complicated historical record of great earthquakes along the Nankai trough (Figure 2). Generally, the potential of seismic occurrence becomes higher when a LSSE occurs, because shear stresses applied to the seismogenic zone around slow slip regions become larger. However, in our model, we cannot simulate the case that the Tokai slow slip grows into a large earthquake. This is because subducted ridges beneath the Tokai region behave as barriers to the growth of LSSEs, and the accumulation speed of shear stress off Kii Peninsula is faster than that in the Tokai region, thus an earthquake tends to initiate there [*Takayama et al*., 2008]. Therefore, we cannot discuss the details of the relation between LSSEs and the anticipated Tokai earthquake in our model. In addition, the preseismic sliding area off Kii Peninsula with l_c = 71 km may be too large. Since plate convergence rates are fast at western parts of the study area [*Heki and Miyazaki*, 2001] and we assume that a constant slip at the plate convergence rate occurs outside the study area, stress easily concentrates at the western edge of study area and seismic rupture tends to start there. To avoid rupture starting from the western edge, we applied enough large L (= 0.13 m). Because our principal objective is to simulate that the Tokai segment did not rupture and LSSEs have recurred beneath

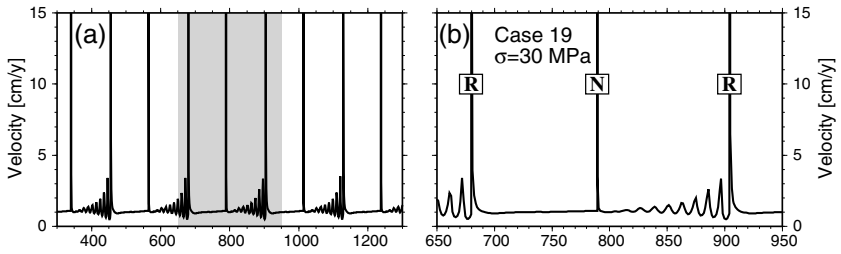

Figure 17. (a,b) Time evolution of slip velocity for case 19 at the location marked by a cross in Figure 3e. The shaded period in Figure 17a is enlarged in Figure 17b. R and N in Figure 17b denote the occurrence of great earthquakes during which the Tokai segment is ruptured and not ruptured, respectively.

Lake Hamana, we applied the same L for all the area except for the Tokai region to simplify the spatial distribution of friction parameters. Therefore, we think that the large preseismic sliding area in this study may be overestimated. The ability to develop simulations that reproduce that complex sequence is important for earthquake prediction and, although it is our final aim, it is beyond the scope of this paper.

5. Conclusions

[35] We extended the study area of *Hirose et al*. [2009] westward to include the western Shikoku region, which allowed us to more realistically simulate the locked state of the plate interface of the Tokai segment. Our 3-D numerical simulations successfully modeled the lack of rupture of the Tokai segment during the 1944 Tonankai earthquake as well as the recurring LSSEs in the Tokai region that precede its rupture. We also found little difference in our simulations of the behavior comparing simulations using two friction laws (the composite law and the slip law).Relatively larger L and σ in areas of subducted ridges than those in other regions are essential to avoid rupture of the Tokai segment during the 1944 Tonankai earthquake because the energy required for rupture increases in proportion to these parameters. Furthermore, the examination of spatial distributions of large L suggests that there may be more subducted ridges deeper beneath the Tokai region than those identified by *Kodaira et al*. [2004]. We found that it is necessary to assign low values of σ and L to the area beneath Lake Hamana in order to reproduce the recurring LSSEs. Low value of σ is consistent with the observations that suggest that the dehydration process is especially active in the subducting slab beneath Lake Hamana [*Hirose et al*., 2008b; *Matsubara et al*., 2008; *Kato et al*., 2010]. The term of a high pore pressure (low effective normal stress) may be the keyword for generating SSEs. The amplitudes of the simulated LSSEs were larger during the periods following great earthquakes without rupture of the Tokai segment because shear stress was increased around the Tokai segment when it was not ruptured. Thus, we concluded that the LSSE observed in the Tokai region during 2001–2005 may reflect concentration of stress related to the arrest of rupture of the Tokai segment during the 1944 Tonankai earthquake.

[36] **Acknowledgments.** We thank Hidemi Ito for the use of his simulation program. We also thank the Hydrographic and Oceanographic Department of the Japan Coast Guard for providing digital bathymetric data. The manuscript was greatly improved by careful reviews of N. Kato and two anonymous reviewers. Figures were prepared using GMT [*Wessel and Smith*, 1991].

References

Ando, M. (1999), General remarks: What should be done in Japan to prepare for the next Nankai earthquake? (in Japanese), *Mon. Chikyu*, *24*, 5–13.

Baba, T., and P. R. Cummins (2005), Contiguous rupture areas of two Nankai Trough earthquakes revealed by high-resolution tsunami waveform inversion, *Geophys. Res. Lett.*, *32*, L08305, doi:10.1029/2004GL022320.

Beeler, N. M., T. E. Tullis, and J. D. Weeks (1994), The roles of time and displacement in the evolution effect in rock friction, *Geophys. Res. Lett.*, *21*, 1987–1990.

Blanpied, M. L., D. A. Lockner, and J. D. Byerlee (1991), Fault stability inferred from granite sliding experiments at hydrothermal conditions, *Geophys. Res. Lett.*, *18*, 609–612.

Central Disaster Management Council (2001), Report of the specialized investigation committee about Tokai earthquake (in Japanese), <http://www.bousai.go.jp/jishin/chubou/20011218/siryou2-2.pdf>, (2006-11-15).

Dieterich, J. H. (1979), Modeling of rock friction, *J. Geophys. Res.*, *84*, 2161–2175.

Dieterich, J. H. (1981), Constitutive properties of faults with simulated gouge, in *Mechanical Behavior of Crustal Rocks: An International Review*, edited by N. L. Carter, M. Freidman, J. M. Logan, and D. W. Stearns, 103–120 pp., Am. Geophys. Union, Washington, D. C.

Earthquake Research Committee (2001), Long-term evaluation of earthquakes in the Nankai trough (in Japanese), <http://www.jishin.go.jp/main/chousa/01sep_nankai/index.htm>, (2006-11-15).

Geographical Survey Institute (2007), Crustal movements in the Tokai district (in Japanese), *Rep. Coord. Comm. Earthquake Predict.*, *77*, 229–312.

Guatteri, M., P. Spudich, and G. C. Beroza (2001), Inferring rate and state friction parameters from a rupture model of the 1995 Hyogo-ken Nanbu (Kobe) Japan earthquake, *J. Geophys. Res.*, *106*, 26,511–26,521.

Hacker, B. R., G. A. Abers, and S. M. Peacock (2003), Subduction factory 1. Theoretical mineralogy, densities, seismic wave speeds, and H_2O contents, *J. Geophys. Res.*, *108*(B1), 2029, doi:10.1029/2001JB001127.

Heki, K., and S. Miyazaki (2001), Plate convergence and long-term crustal deformation in Central Japan, *Geophys. Res. Lett.*, *28*, 2313–2316.

Hirose, F., J. Nakajima, and A. Hasegawa (2008a), Anomalous depth distribution of deep low-frequency earthquakes at the northeast Tokai district, 7th UJNR Earthq. Res. Panel Meet., 90.

Hirose, F., J. Nakajima, and A. Hasegawa (2008b), Three-dimensional seismic velocity structure and configuration of the Philippine Sea slab in southwestern Japan estimated by double-difference tomography, *J. Geophys. Res.*, *113*, B09315, doi:10.1029/2007JB005274.

Hirose, F., K. Maeda, and H. Takayama (2009), An attempt at simulation of long term slow slip events and seismic cycle in the Tokai region (in Japanese with English abstract), *J. Seism. Soc. Jpn.*, *2*(62), 67–84.

Honkura, Y., Y. Nagaya, and H. Kuroki (1999), Effects of seamounts on an interplate earthquake at the Suruga trough, Japan, *Earth Planets Space*, *51*, 449–454.

Hori, T. (2006), Mechanisms of separation of rupture area and variation in time interval and size of great earthquakes along the Nankai Trough, southwest Japan, *J. Earth Simul.*, *5*, 8–19.

Hori, T., N. Kato, K. Hirahara, T. Baba, and Y. Kaneda (2004), A numerical simulation of earthquake cycles along the Nankai Trough in southwest Japan: lateral variation in frictional property due to the slab geometry controls the nucleation position, *Earth Planet. Sci. Lett.*, *228*, 215–226.

Hyndman, R. D., K. Wang, and M. Yamano (1995), Thermal constraints on the seismogenic portion of the southwestern Japan subduction thrust, *J. Geophys. Res.*, *100*, 15,373–15,392.

Ichinose, G. A., H. K. Thio, P. G. Somerville, T. Sato, and T. Ishii (2003), Rupture process of the 1944 Tonankai earthquake (M_s8.1) from the inversion of teleseismic and regional seismograms, *J. Geophys. Res.*, *108*(B10), 2497, doi:10.1029/2003JB002393.

Ishibashi, K. (1976), Reexamination of anticipated great earthquake in Tokai district, -Suruga Bay great earthquake- (in Japanese), Prog. Abst. Seism. Soc. Jpn., 1976, Fall Meet., 30-34.

Kanamori, H. (1977), The energy release in great earthquakes, *J. Geophys. Res.*, *82*, 2981–2987.

Kato, N. (2004), Interaction of slip on asperities: Numerical simulation of seismic cycles on a two-dimensional planar fault with nonuniform frictional property, *J. Geophys. Res.*, *109*, B12306, doi:10.1029/2004JB003001.

Kato, N., and T. E. Tullis (2001), A composite rate- and state-dependent law for rock friction, *Geophys. Res. Lett.*, *28*, 1103–1106.

Kato, N., and T. E. Tullis (2003), Numerical simulation of seismic cycles with a composite rate- and state-dependent friction law, *Bull. Seism. Soc. Am.*, *93*, 841–853.

Kato, A., et al. (2010), Variations of fluid pressure within the subducting oceanic crust and slow earthquakes, *Geophys. Res. Lett.*, *37*, L14310, doi:10.1029/2010GL043723.

Kikuchi, M., M. Nakamura, and K. Yoshikawa (2003), Source rupture processes of the 1944 Tonankai earthquake and the 1945 Mikawa earthquake derived from low-gain seismograms, *Earth Planets Space*, *55*, 159–172.

Kimata, F., and T. Yamauchi (1998), Time series of line lengths on the baselines in the Tokai region detected by EDM in the period of 1978 to 1997, (in Japanese), *J. Seism. Soc. Jpn.*, *2*(51), 229–232.

Kobayashi, A., and T. Yamamoto (2011), Repetitive long-term slow slip events beneath the Bungo Channel, southwestern Japan, identified from leveling and sea level data from 1979 to 2008, *J. Geophys. Res.*, *116*, B04406, doi:10.1029/2010JB007822.

Kobayashi, A., and A. Yoshida (2004), Recurrence of the Tokai slow slip inferred from the tide gauge data at Maisaka (in Japanese with English abstract), *J. Geodetic Soc. Jpn.*, *50*, 209–212.

Kobayashi, T., M. Hashimoto, and T. Tabei (2006), Estimate of interplate coupling along the Nankai trough, southwest Japan, using a new plate interface model, American Geophysical Union Fall Meeting 2006, S43D-07.

Kodaira, S., T. Iidake, A. Kato, J. Park, T. Iwasaki, and Y. Kaneda (2004), High pore fluid pressure may cause silent slip in the Nankai Trough, *Science*, *304*, 1295–1298.

Kuroki, H., H. M. Ito, and A. Yoshida (2002), A three-dimensional simulation of crustal deformation accompanied by subduction in the Tokai region, central Japan, *Phys. Earth Planet. Inter.*, *132*, 39–58, doi:10.1016/S0031-9201(02)00043-2.

Kuroki, H., H. Ito, H. Takayama, and A. Yoshida (2004), 3-D simulation of the occurrence of slow slip events in the Tokai region with a rate- and state-dependent friction law, *Bull. Seism. Soc. Am.*, *94*, 2037–2050.

Liu, Y., and J. R. Rice (2005), Aseismic slip transients emerge spontaneously in three-dimensional rate and state modeling of subduction earthquake sequences, *J. Geophys. Res.*, *110*, B08307, doi:10.1029/2004JB003424.

Liu, Y., and J. R. Rice (2007), Spontaneous and triggered aseismic deformation transients in a subduction fault model, *J. Geophys. Res.*, *112*, B09404, doi:10.1029/2007JB004930.

Matsubara, M., K. Obara, and K. Kasahara (2008), High-Vp/Vs zone accompanying non-volcanic tremors and slow-slip events beneath southwestern Japan, *Tectonophysics*, *472*, 6–17, doi:10.1016/j.tecto.2008.06013.

Matsuzawa, T., H. Hirose, B. Shibazaki, and K. Obara (2010), Modeling short- and long-term slow slip events in the seismic cycles of large subduction earthquakes, *J. Geophys. Res.*, *115*, B12301, doi:10.1029/2010JB007566.

Miyazaki, S., P. Segall, J. J. McGuire, T. Kato, and Y. Hatanaka (2006), Spatial and temporal evolution of stress and slip rate during the 2000 Tokai slow earthquake, *J. Geophys. Res.*, *111*, B03409, doi:10.1029/2004JB003426.

Miyoshi, T., and K. Ishibashi (2004), Geometry of the seismic Philippine Sea slab beneath the region from Ise bay to western Shikoku, southwest Japan (in Japanese with English abstract), *J. Seism. Soc. Jpn.*, *2*(57), 139–152.

Mura, T. (1987), *Micromechanics of defects in solids*, Martinus Nijhoff Publishers, Dordrecht, The Netherlands, 2nd edition, pp. 587.

Nakatani, M. (2001), Conceptual and physical clarification of rate and state friction: Frictional sliding as a thermally activated rheology, *J. Geophys. Res.*, *106*, 13,347–13,380.

National Research Institute for Earth Science and Disaster Prevention (2004), The slow slip event in the Tokai region, detected by tilt and seismic observation—Possible reccurence—(in Japanese), *Rep. Coord. Comm. Earthquake Predict.*, *71*, 584–587.

Noguchi, S. (1996), Geometry of the Philippine Sea slab and the convergent tectonics in the Tokai district, Japan (in Japanese with English abstract), *J. Seism. Soc. Jpn.*, *2*(49), 295–325.

Ohta, Y., F. Kimata, and T. Sagiya (2004), Reexamination of the interplate coupling in the Tokai region, central Japan, based on the GPS data in 1997–2002, *Geophys. Res. Lett.*, *31*, L24604, doi:10.1029/2004GL021404.

Okino, K., Y. Shimakawa, and S. Nagaoka (1994), Evolution of the Shikoku Basin, *J. Geomagn. Geoelectr.*, *46*, 463–479.

Ozawa, K., and T. Sagiya (2008), Kinematic modeling of crustal deformation in the Central Japan, Proceeding of the 7th General Assembly of Asian Seismological Commission and the 2008 Fall meeting of Seismological Society of Japan, Y4-205.

Ozawa, S., M. Murakami, M. Kaidzu, T. Tada, T. Sagiya, Y. Hatanaka, H. Yarai, and T. Nishimura (2002), Detection and monitoring of ongoing aseismic slip in the Tokai region, central Japan, *Science*, *298*, 1009–1012.

Press, W. H., S. A. Teukolsky, W. T. Vetterling, and B. P. Flannery (1992), *Numerical Recipes in Fortran*, 2nd ed., pp., 963, Cambridge Univ. Press, Cambridge, England.

Rice, J. R. (1992), in *Fault Stress States, Pore Pressure Distributions, and the Weakness of the San Andreas Fault, in Fault Mechanics and Transport Properties of Rocks*, edited by B. Evans, and T.-F. Wong, 475–503 pp., Academic Press, San Diego, Calif., USA.

Rice, J. R. (1993), Spatio-temporal complexity of slip on a fault, *J. Geophys. Res.*, *98*, 9885–9907.

Rubin, A. M. (2008), Episodic slow slip events and rate-and-state friction, *J. Geophys. Res.*, *113*, B11414, doi:10.1029/2008JB005642.

Rubin, A. M., and J.-P. Ampuero (2005), Earthquake nucleation on (aging) rate and state faults, *J. Geophys. Res.*, *110*, B11312, doi:10.1029/2005JB003686.

Ruina, A. (1983), Slip instability and state variable friction laws, *J. Geophys. Res.*, *88*, 10,359–10,370.

Sagiya, T., A. Oishi, R. Miyajima, K. Ishikawa, M. Ohzono, and K. Ozawa (2007), Spatio-temporal variation of plate interactions in the Tokai district as viewed from leveling data (2), Abst. Jpn. Geosci. Union Meet., 2007, T234-010.

Seno, T., T. Sakurai, and S. Stein (1996), Can the Okhotsk plate be discriminated from the North American plate?, *J. Geophys. Res.*, *101*, 11,305–11,315.

Takayama, H., K. Maeda, and F. Hirose (2008), Effect of the plate boundary configuration on the initiation point of great earthquakes along the Nankai trough (in Japanese), *J. Seism. Soc. Jpn.*, *2*(60), 279–284.

Tse, S. T., and J. R. Rice (1986), Crustal earthquake instability in relation to the depth variation of frictional slip properties, *J. Geophys. Res.*, *91*, 9452–9472.

Tsuji, Y. (1999), Nankai earthquake and a tsunami associated with it (in Japanese), extra edition of Monthly Chikyu, 24, 36–49.

Wessel, P., and W. H. F. Smith (1991), Free software helps map and display data, *EOS Trans. AGU*, *72*, 441.

Yang, H., Y. Liu, and J. Lin (2012), Effects of subducted seamounts on megathrust earthquake nucleation and rupture propagation, *Geophys. Res. Lett.*, *39*, L24302, doi:10.1029/2012GL053892.

Zhang, H., and C. H. Thurber (2003), Double-difference tomography: The method and its application to the Hayward Fault, California, *Bull. Seism. Soc. Am.*, *93*, 1875–1889.